

# A Tailorable Series of Elastomeric-To-Rigid, Selfhealable, Shape Memory Bismaleimide

Yuejia Li, Fenghua Zhang,\* Yanju Liu, and Jinsong Leng\*

In recent years, there has been rapid development in the field of shape memory materials with active deformation performance. However, bismaleimide, a widely used thermosetting material in aerospace, has been largely overlooked in shape memory applications. This work presents the synthesis of a molecule containing an alkene bond adjacent to an oxygen atom. Through molecular design, a one-time reaction between this specialized molecule and the bismaleimide molecule is successfully achieved, facilitated by the steric hindrance effect. Therefore, a new series of shape memory bismaleimide materials are obtained. By introducing a diamine to adjust the chain length, the properties of material are further improved, resulting in increasing static modulus by 506 times. The synthesized materials exhibit a broad glass transition temperature ( $T_g$ ) range exceeding 153 °C, remarkable stiffness tunability. Notably, in the synthesis process of this materials series, the disulfide bonds are introduced, which facilitates the realization of self-healing and reprocessable functionalities in the resulting thermosetting materials. This significant advancement lays a solid foundation for the future recycling and reuse of aircraft, satellites, and other equipment, offering promising prospects for enhancing sustainability and efficiency within the aerospace industry.

commonly employed thermosetting material in engineering applications, exhibits superior mechanical properties, elevated transition temperatures, as well as enhanced heat resistance and thermal stability, surpassing those of thermoplastic materials. Consequently, BMI finds indispensable utility in aerospace domains encompassing self-deployable structures and morphing aircraft.<sup>[2]</sup> Thus, the development of high-performance thermosetting BMI materials incorporating shape memory effects assumes paramount research significance, offering considerable potential for advancing the applications of SMPs.

BMI is a high-performance thermosetting polymer that offers several advantages, particularly in the aerospace materials domain. BMI resins exhibit comparable flowability and moldability to typical thermosetting resins. Upon reaching temperatures exceeding 180 °C, BMI monomers undergo self-polymerization, resulting in the formation of a 3D network structure. The high degree of cross-linking in these materials contributes to their exceptional high-

temperature performance. However, this feature also presents a significant drawback, as cured BMI polymers tend to exhibit brittleness and low fracture toughness. While similar challenges exist in other thermosetting polymers, such as multifunctional epoxy resins, the presence of polar carbonyl groups in BMI resins exacerbates these issues by limiting polymer chain ordering and energy dissipation opportunities. To enhance the toughness and processability of BMI resins, various approaches are employed, including blending them with other thermosetting materials such as cyanate esters,<sup>[2a,3]</sup> epoxies,<sup>[4]</sup> and diamines.<sup>[2a,5]</sup> Through the incorporation of these additives and subsequent reactions with BMI, improvements in material toughness, enhanced dielectric properties, reduced moisture absorption, and enhanced liquid processability can be achieved. Allyl compounds, known for their inherent stability, are commonly used as co-monomers with BMI due to their limited self-polymerization even at elevated temperatures. Consequently, they are well-suited for copolymerization with BMI. By engaging in ene reactions with allyl compounds, BMI can undergo chain extension, forming intermediate structures reminiscent of styrene. These intermediates readily participate in Diels–Alder reactions with BMI, resulting in enhanced toughness. Notably, di-allyl bisphenol A represents an early allyl compound employed for BMI modification.<sup>[6]</sup> Its

## 1. Introduction

Shape memory polymers (SMPs) are a unique class of stimuli-responsive polymers that possess the ability to program and fix temporary shapes, which can be subsequently recovered to their original configurations under specific external stimuli.<sup>[1]</sup> As intelligent materials capable of autonomous deformation, SMPs offer advantageous features such as lightweight nature, low cost, ease of processing, controllable shape-changing performance, and tunable transition temperatures. Bismaleimide (BMI), a

Y. Li, F. Zhang, J. Leng  
Centre for Composite Materials and Structures  
Harbin Institute of Technology (HIT)  
No.2 Yikuang Street, P.O. Box 3011, Harbin 150080, P. R. China  
E-mail: zhangfenghua@hit.edu.cn; lengjs@hit.edu.cn

Y. Liu  
Department of Astronautical Science and Mechanics  
Harbin Institute of Technology (HIT)  
No. 92 West Dazhi Street, P.O. Box 301, Harbin 150001, P. R. China

 The ORCID identification number(s) for the author(s) of this article can be found under <https://doi.org/10.1002/sml.202307244>

DOI: 10.1002/sml.202307244

advantages lie in its cost-effectiveness, favorable flow characteristics upon heating, and compatibility with BMI, leading to improved toughness properties in the resulting materials.

Permanent crosslinked materials exhibit exceptional mechanical properties and solvent resistance; however, once synthesized, they cannot be processed or reshaped. On the other hand, non-crosslinked polymers and polymers with reversible crosslinking are processable but tend to be soluble. Thermosetting polymers find extensive applications in coatings, adhesives, electrical/electronic components, and composites owing to their remarkable mechanical strength, heat resistance, and chemical stability. Nevertheless, conventional thermosetting materials with stable covalent bond networks lack the ability to be reshaped, reprocessed, or dissolved, posing significant challenges for recycling and repair efforts. Consequently, there is a pressing need to address these limitations for the sake of sustainable development. In recent years, a significant breakthrough has been made by introducing dynamic covalent bonds into thermosetting networks. This approach has enabled the reprocessing of traditional thermosetting polymers, such as crosslinked epoxy resin<sup>[7]</sup> and polyurethane,<sup>[8]</sup> through hot pressing. Bismaleimide resin, a high-performance thermosetting addition polyimide, is widely employed as the matrix resin for multilayer printed circuit boards and advanced composites in the aerospace industry.<sup>[2b,9]</sup> The critical thermosetting bismaleimide resin system in the industry mainly comprises BMI and 2,2'-diallyl bisphenol A,<sup>[2b,10]</sup> as well as BMI and 4,4'-diaminodiphenylmethane,<sup>[9,11]</sup> which undergo thermal curing via maleimide/allyl reaction and maleimide/amine Michael addition reaction, respectively.<sup>[12]</sup> Three decades ago, Sastri et al. reported a recyclable thermosetting bismaleimide resin system composed of 4,4'-bismaleimide disulfide and 4-aminophenyl disulfide (also known as 4,4'-dithioline) or 4,4'-diaminodiphenylmethane.<sup>[13]</sup>

Currently, self-healing/reshapeable materials are predominantly found in the form of soft materials, making it challenging to achieve self-healing/reshapeability in rigid materials. Consequently, the development of rigid, self-healing/reshapeable materials holds tremendous significance. Self-healing/reshaping is usually achieved through dynamically changing bonds between polymer chains, such as ester bonds,<sup>[14]</sup> urea bonds,<sup>[15]</sup> and disulfide bonds.<sup>[16]</sup> The disulfide bond has the advantage of higher energy, which helps to improve the mechanical properties of the material and can provide self-healing caused by different stimuli, achieving more functions.<sup>[17]</sup> Yue Lai et al. introduced disulfide bonds in polyurethane to achieve excellent tensile properties of the material (stress of 25 MPa, strain of 1600%), while also achieving self-healing of the material.<sup>[18]</sup> Thermosetting SMPs commonly exhibit shape memory effects by programming temporary shapes that can be subsequently restored to their permanent shapes. This shape memory transition relies on the fixed phase of network cross-linking points as well as the reversible deformation phase of intercrosslinked molecular chains, which involves alterations in the chain conformation of the reversible deformation phase. Thermosetting SMPs typically possess high hardness and lack the capability for material restructuring or reshaping. During service in complex environments, SMP materials unavoidably experience damage, such as microcracks, leading to a substantial reduction in mechanical performance, shortened service life, and compromised safety. Reducing the amount

of materials brought into space can reduce the pressure of transportation in space, and it is of great significance to use the pristine materials for remolding and realizing their shape memory function as the way it was. Consequently, the development of thermosetting shape memory resin systems capable of achieving reshaping with prolonged service life and enhanced safety is of utmost importance.

In this study, we synthesized a thermosetting BMI material with shape memory properties. By strategically designing the molecular structure, we introduced a molecule with an alkene bond adjacent to an oxygen atom, which exhibited spatial hindrance effects during the reaction with BMI. This resulted in a reduced cross-linking density and the formation of a shape memory material. Further enhancements were achieved by incorporating a diamine, leading to a secondary reaction of the maleimide groups. This decreased the cross-linking density and increased the chain length. The resulting materials within the same series displayed impressive properties, including a 506-fold change in static modulus and a wide range of  $T_g$  exceeding 153 °C. These materials offer tunable stiffness and deformation performance at different transition temperatures. This is called elastic-to-rigid performance, where the characteristics of materials with elastic performance are Young's modulus between 0.1 and 10 MPa and high elongation >200%.<sup>[19]</sup> Moreover, we introduced disulfide bonds during the synthesis process of the molecules containing two alkene bonds, enabling the thermosetting material to possess self-healing and reprocess functionalities. This advancement holds great promise for applications in recycling and reusing aerospace equipment.

## 2. Results and Discussion

Figure 1a,b show the reaction equation for synthesizing 4,4'-diallyloxydiphenyldisulfide (DPS) and the infrared spectra of it. The absorption peak of the hydroxyl group at 3300–3400  $\text{cm}^{-1}$  has disappeared, while absorption peaks corresponding to aromatic and olefinic C-H stretching vibrations appear at 3080, 3020, and 2975  $\text{cm}^{-1}$ . The stretching vibration absorption peak of the carbon-carbon double bond ( $\nu \text{C}=\text{C}$ ) is observed at 1615  $\text{cm}^{-1}$ , and the bending vibration absorption peak ( $\delta \text{C}=\text{C}$ ) appears at 994 and 938  $\text{cm}^{-1}$ . The absorption peaks of the bromoalkane disappear below 600  $\text{cm}^{-1}$ , while the absorption peak of the disulfide bond remains at 539  $\text{cm}^{-1}$ . The absorption of the aromatic ether bond ( $\nu \text{Ar}-\text{O}-\text{C}$ ) is reflected near 1262  $\text{cm}^{-1}$ , and the absorption peaks of the aromatic ring skeleton are distributed at 1595 and 1498  $\text{cm}^{-1}$ . The absorption peak at 844  $\text{cm}^{-1}$  corresponds to  $\delta \text{Ar}-\text{H}$ . These observations confirm the structural characteristics of the synthesized monomer.<sup>[20]</sup> Thus, it can be concluded that the DPS with the structure shown in Figure 1a has been successfully synthesized. By strategically designing the molecular structure, disulfide bonds are introduced into the DPS with diene bonds.

Infrared spectroscopy provides a qualitative analysis of the monomer structure, while nuclear magnetic resonance (NMR) spectroscopy allows for a quantitative analysis and determination of the bonding modes in the monomer structure. Deuterated chloroform ( $\text{CDCl}_3$ ) was used as the solvent, and tetramethylsilane (TMS) was used as the internal standard. The  $^1\text{H}$ -NMR spectrum of the synthesized monomer is shown in Figure 1c, and

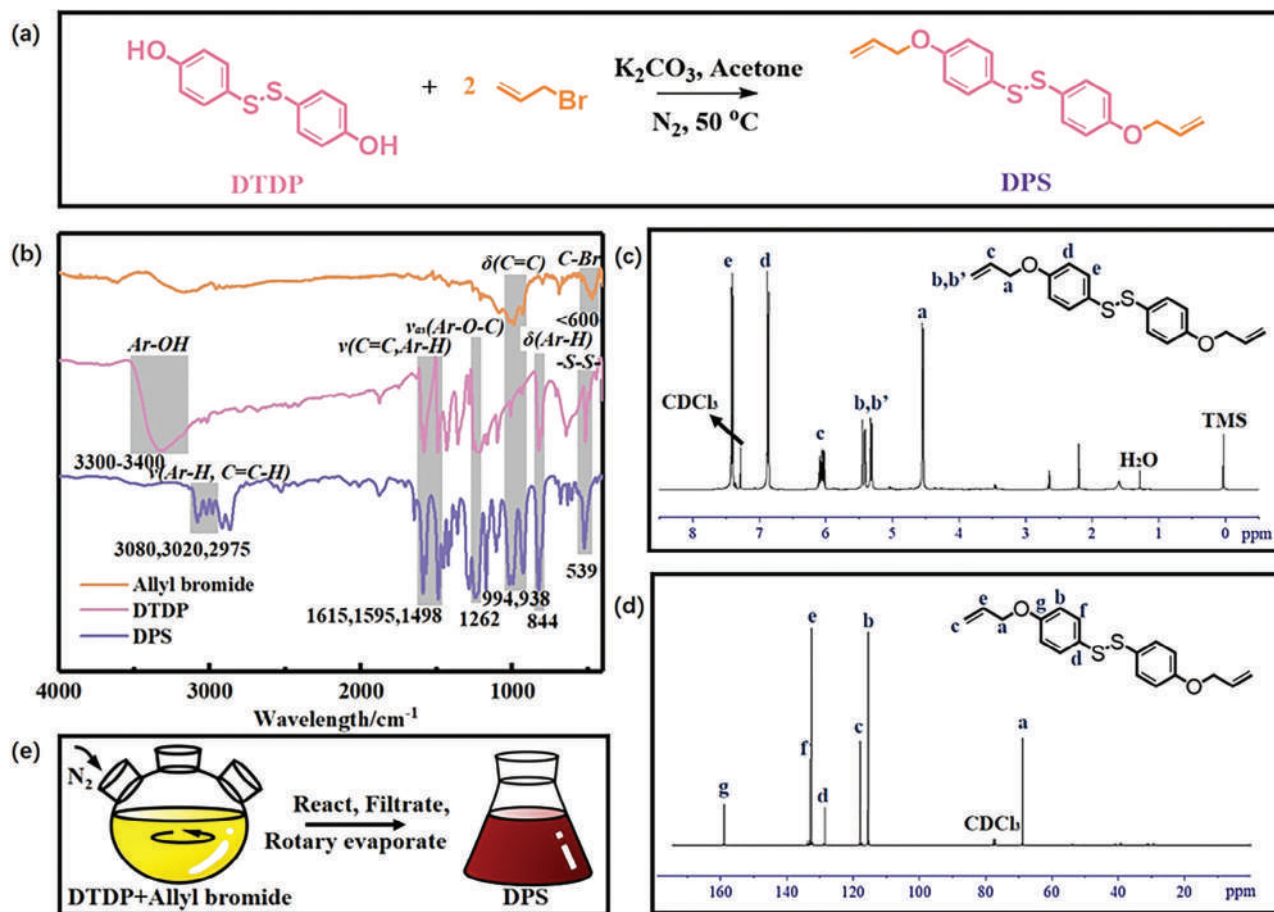


**Figure 1.** a) The process of Bis(4-hydroxyphenyl) disulfide (DTDP) reacting with Allyl bromide; b) FT-IR spectra of reactant DTDP, Allyl bromide, and product DPS; c)  $^1H$ -NMR spectra of DPS, d)  $^{13}C$ -NMR spectra of DPS; e) Schematic diagram of reaction process and color changes.

the  $^{13}C$ -NMR spectrum is shown in Figure 1d. In Figure 1c, the absorption peak at  $\delta = 7.28$  corresponds to the solvent  $CDCl_3$ . Due to the molecular structure's symmetry, only five sets of resonances corresponding to the monomer structure are observed in the spectrum. They are as follows:  $\delta_a = 4.55, 4.54$ ;  $\delta_b = 5.45, 5.41, 5.33, 5.30$ ;  $\delta_c = 6.11, 6.10, 6.08, 6.07, 6.05, 6.04, 6.03, 6.01$ ;  $\delta_d = 6.88, 6.86$ ;  $\delta_e = 7.42, 7.40$ . The peak splitting pattern is consistent with the monomer structure. The integration areas of each peak can be used to calculate the relative number of hydrogen atoms, which matches the distribution of hydrogen atoms in the molecular structure. In Figure 1d, the absorption peak at  $\delta = 70.1$  corresponds to the solvent  $CDCl_3$ . Similarly, due to the molecular structure's symmetry, only seven sets of resonances corresponding to the monomer structure are observed in the spectrum. They are as follows:  $\delta_a = 68.9$ ;  $\delta_b = 115.5$ ;  $\delta_c = 117.9$ ;  $\delta_d = 128.6$ ;  $\delta_e = 132.5$ ;  $\delta_f = 133.0$ ;  $\delta_g = 159.0$ . The quantitative analysis using  $^1H$ -NMR and  $^{13}C$ -NMR spectroscopy confirms the structure of the synthesized monomer.<sup>[21]</sup> The reaction process and the colors of reactants and products were illustrated in Figure 1e.

The obtained DPS and 4,4'-bismaleimideodiphenylmethane (BDM) are mixed and heated for pre-polymerization, and the cured material is named DPS1. The schematic diagram of the reaction between BDM and DPS is shown in Figure 2a. The resulting products of the reaction are depicted. The reaction between

the diene and BDM proceeds only once, as the presence of an ether bond introduces spatial hindrance, preventing subsequent reactions and lowering the crosslinking density, thus enabling the material to exhibit shape memory effects. The crosslinking density comparison between the product obtained from traditional reactions as a "contrast" and DPS1 are shown by the swelling test results in Figure S1 (Supporting Information). In both water and organic solvents, the swelling degree of DPS1 are lower than that of "contrast", indicating that the crosslinking density of DPS1 has decreased. Highlighting that conventional diene-BDM reactions typically undergo secondary reactions, resulting in excessive crosslinking density and the absence of shape memory effects, as shown in Figure S2 (Supporting Information). In the first step, the double bond of the bismaleimide group undergoes opening by reacting with the diene, while in the second step, the addition of a diamine allows for further reaction between the amine and the bismaleimide group, as shown in Figure 2b. The curing materials with a molar ratio of 25%, 50%, 75%, and 100% diamine are named DPS2, DPS3, DPS4, and DPS5, respectively. This complete opening of the bismaleimide double bond leads to the formation of elongated chain molecules, which in turn results in a sharp decrease in modulus and a significant increase in fracture elongation for the obtained material, yielding remarkable effect of reducing modulus. Materials with

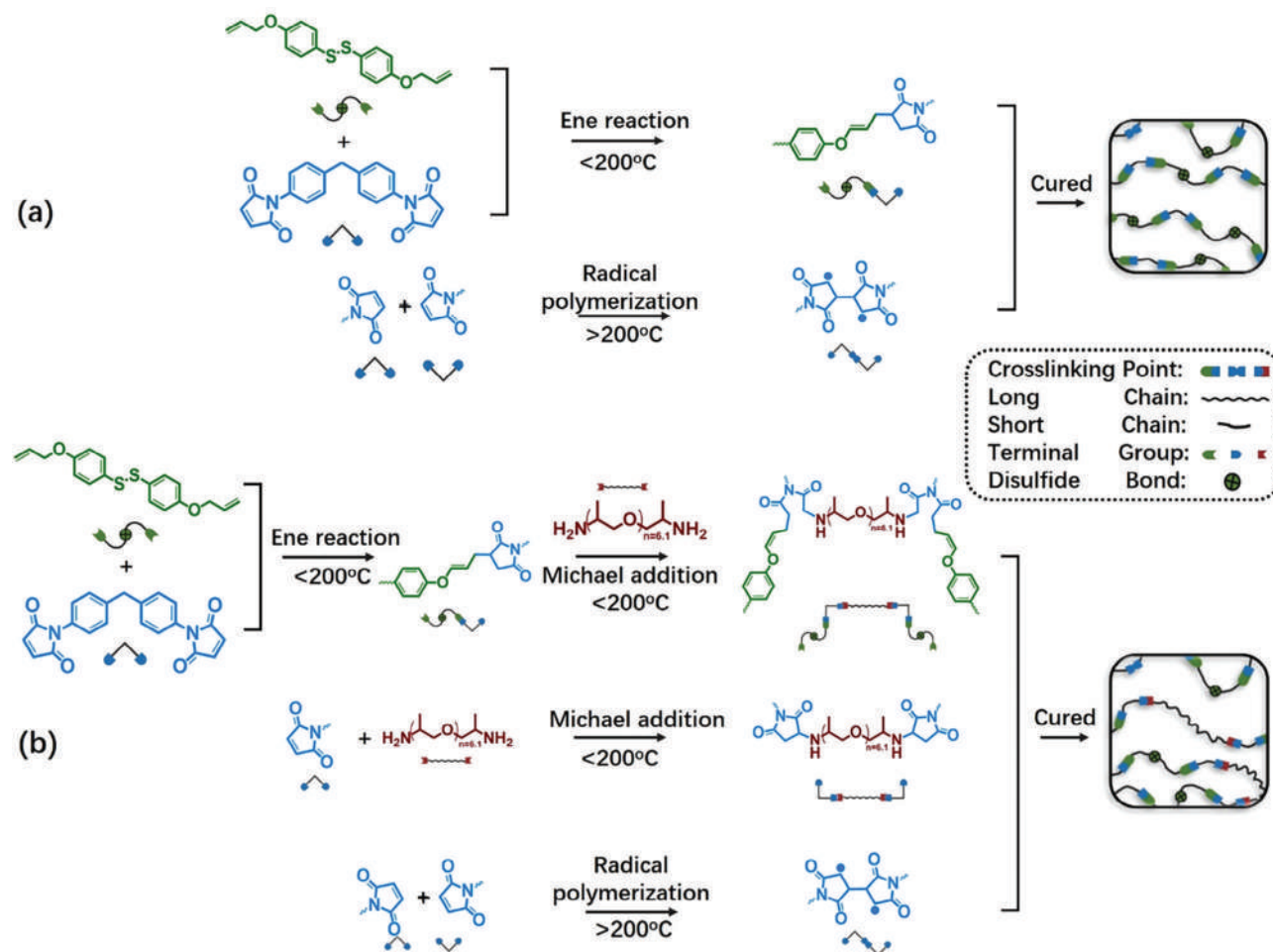


**Figure 2.** The reaction process of resin system, a) BDM+DPS, b) BDM+DPS+D400.

lower modulus exhibited lower crosslinking density, which was characterized through swelling test results in Figure S1 (Supporting Information). Additionally, the introduction of the diene allyl ether in the first step reaction introduces spatial hindrance, contributing to the modulation of the material's modulus. Among them, the circular shapes with an "X" in the center indicate the presence of self-healing functionality, while the circular shapes without an "X" do not possess self-healing performance, as shown in Figure S1 (Supporting Information).

From **Figure 3a**, the structural characteristics of the synthesized product were confirmed through Fourier Transform (FTIR) analysis. After the reaction, the maleimide groups were transformed into succinimide groups. The asymmetric stretching vibration peak of the C—N—C bond in the maleimide group (vas peak at  $1148\text{ cm}^{-1}$ ) shifted to  $1180\text{ cm}^{-1}$  in the succinimide group. The deformation peaks of the maleimide ring shifted to the right at  $1396$  and  $687\text{ cm}^{-1}$ . The out-of-plane bending peak of the =C—H group and the stretching vibration peak of —C=O at  $829$  and  $1709\text{ cm}^{-1}$ , respectively, which are characteristic of the maleimide group, remained unchanged.<sup>[22]</sup> The trans-stretching vibration peak of the ether bond between the DPS monomer and the reaction product can be observed at  $1240\text{ cm}^{-1}$ , indicating no change before and after the reaction.<sup>[23]</sup> The scissoring vibra-

tion peak of the primary amine (—NH<sub>2</sub>) group, located at  $1622\text{ cm}^{-1}$ , disappeared, while the secondary amine groups gradually increased, resulting in a broader and smoother stretching peak observed at  $3350\text{ cm}^{-1}$  as shown in Figure S3 (Supporting Information). These observations confirm the structural characteristics of the cured resin.<sup>[22]</sup> The heating and heat release curves of the prepolymer are shown in Figure S4 (Supporting Information).

The rheological behavior of different formulation materials at different temperatures was characterized using rheological tests. As shown in Figure 3b, the resins DPS1 – DPS4 exhibited a trend of initially decreasing viscosity followed by increasing viscosity during the temperature ramp. The DPS1 – DPS5 material is in an oligomer state when not cured. At low temperatures at room temperature, the resin exhibits poor flowability and high viscosity. The addition of flexible molecule D400 reduces the viscosity of DPS2 – DPS5 resin compared to DPS1 resin, and DPS2 – DPS5 exhibits a flowing state at room temperature. This results in DPS1 exhibiting a narrower processing window than DPS2 – DPS5. In lower temperatures range, the resin absorbs heat during the heating process, resulting in a higher fluidity of the material and the viscosity of the resins decreased significantly with increasing temperature. The viscosity values of different

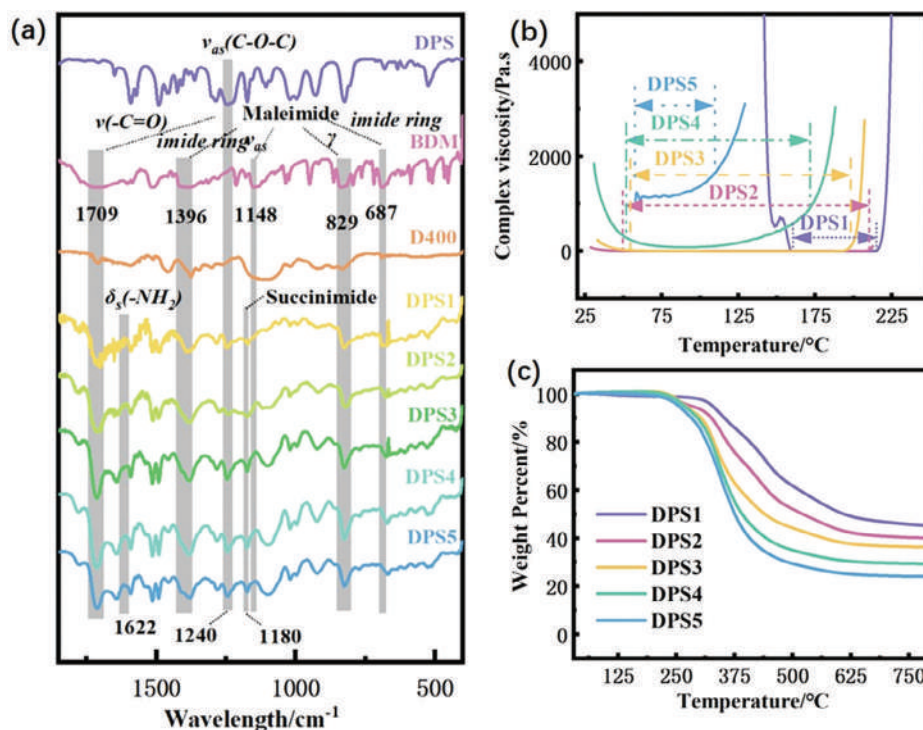


**Figure 3.** a) FT-IR spectra of DPS, BDM, D400, and DPS1-DPS5; b) Temperature-viscosity curves of prepolymers with different concentrations of D400; c) thermogravimetric test curves of SMP materials with different D400 contents in nitrogen atmosphere.

prepolymers increased with increasing reactant concentration, resulting in higher minimum viscosity values. Further temperature increase and higher D400 content accelerated the reaction, leading to an increase in the minimum viscosity values. The temperature range at which the material exhibited low viscosity is referred to as the processing window. The processing window widths were all above 35 °C, with the widest reaching 130 °C. This indicates that materials with different ratios exhibited good processability.

The thermal stability of the material was investigated using thermogravimetric analysis (TGA). The thermal decomposition temperature (<5%) was employed to characterize the temperature range suitable for material utilization and determine the residual carbon content. As shown in Figure 3c and Figure S5 (Supporting Information), the thermal decomposition temperatures of the material under both N<sub>2</sub> and air atmospheres were above 250 °C, which exceeded the material's deformation temperature. This indicates that the material can be safely used at the deformation temperature and can undergo self-healing operations safely in air, demonstrating excellent oxygen stability. Among them, the residual carbon content under N<sub>2</sub> atmosphere ranged from 24% to 45%. Materials with higher D400 content exhibited lower residual carbon content and higher decomposition rates. This can be attributed to the longer molecular chain segments, fewer cross-linking points, and higher linear segment proportion in materials with higher D400 content, leading to lower residual carbon content after decomposition. Under the air atmosphere, the initial weight loss of the material was due to the decomposition of the cross-linked network, forming char. Subsequent weight loss was caused by the ox-

idative decomposition of the char layer. The residual carbon content of all material compositions under the air atmosphere was ≈1%.

The dynamic mechanical analysis (DMA) was conducted to evaluate the room temperature (*R.T.*) dynamic modulus, high-temperature dynamic modulus, and glass transition temperature of the materials. The DMA curves of materials with different D400 ratios are shown in Figure 4. Figure 4a illustrates that the storage modulus of materials with different compositions decreases with increasing temperature, indicating the occurrence of glass transition and shape memory behavior. At 30 °C, DPS1 exhibits the highest dynamic modulus of 4118 MPa, which is 66 times higher than the lowest modulus of DPS5 at 62 MPa. The incorporation of D400 leads to a drastic reduction in the dynamic modulus of the materials, transitioning from a rigid to an elastic macroscopic behavior. This is attributed to the opening of the bismaleimide groups induced by D400, resulting in a significant increase in the length of molecular chain segments and a consequent decrease in the modulus of the materials. The comparison of their modulus at high temperature and room temperature is shown in Table S1 (Supporting Information), showing a modulus change of >10 times, indicating that these materials have shape memory properties. Figure 4b presents the temperature-dependent loss factor ( $\tan \delta - T$  curve) for materials with different compositions. The peak of the  $\tan \delta$  curve corresponds to the  $T_g$  of the materials. DPS5 exhibits the lowest  $T_g$  at 42 °C, while DPS1 has the highest  $T_g$  at 195 °C. The materials with different formulations demonstrate a  $T_g$  span of over 150 °C, enabling deformation at different temperatures. The loss factor represents the viscoelastic properties of the material. The higher the

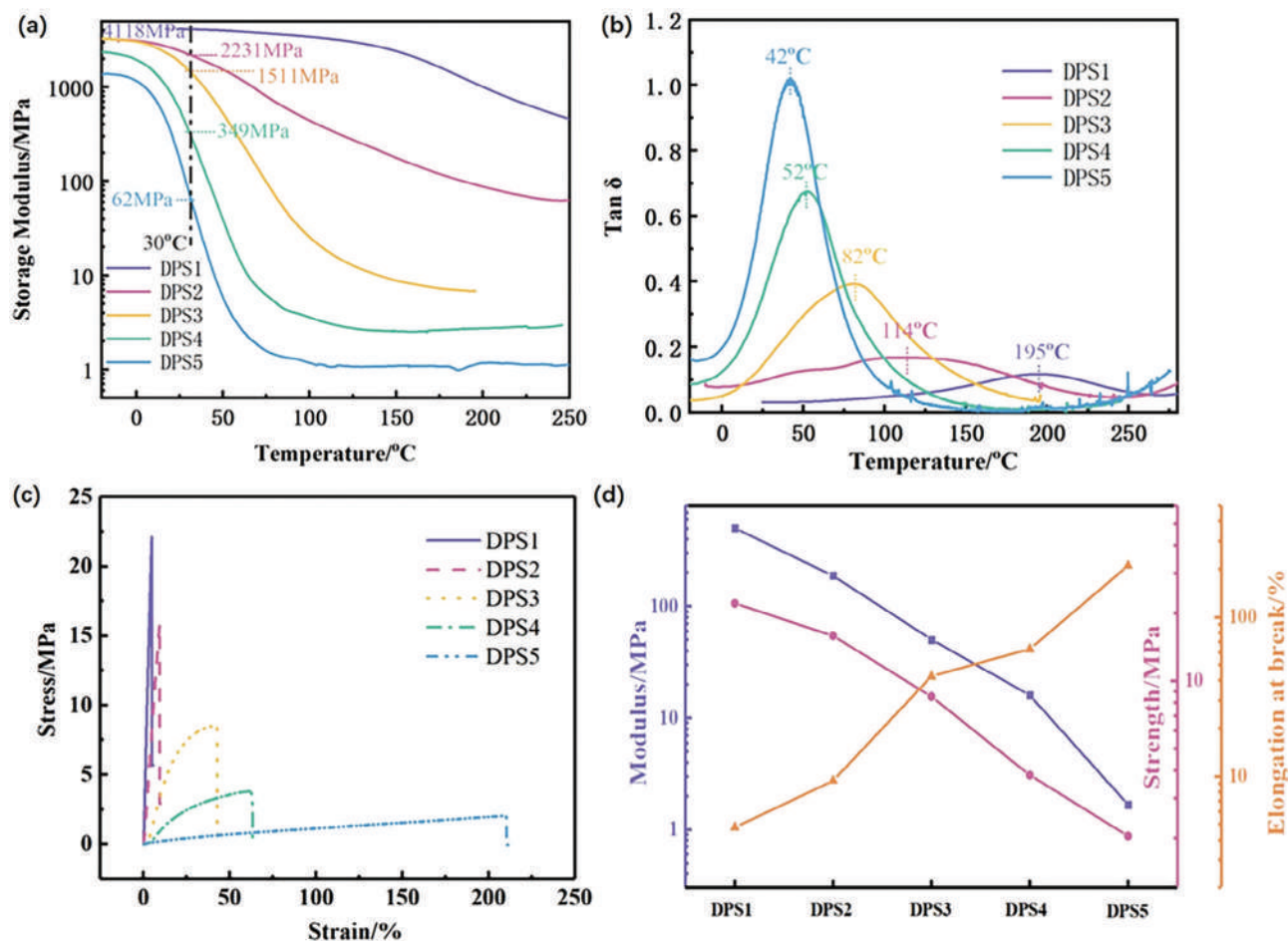


**Figure 4.** Mechanical properties of SMPs: a) DMA Storage Modulus – Temperature curves of materials with different D400 ratios; b) DMA Tan  $\delta$  – T curves of SMPs; c) Tensile stress–strain curves of DPS1 – DPS5; d) Modulus, strength, and fracture elongation data (coordinate axis scale is exponential).

loss factor of DPS5, the greater the viscosity of the material. The lower the loss factor of DPS1, the greater the elasticity of the material. The fixity and recovery ratios of DPS1 – DPS5 were determined through DMA cyclic testing, as shown in Figure 5a–e. The calculated fixing ratios and recovery ratios are summarized in Figure 5f and Table S2 (Supporting Information). DPS1 – DPS4 exhibit fixity ratios above 96%. Although the fixity ratio of DPS5 is slightly lower than 90%, its recovery ratio exceeds 95%. All the mentioned materials demonstrate good fixity and recovery ratios in shape memory cycling, with excellent repeatability.

The mechanical properties of the materials were characterized using static tensile testing at *R.T.* Figure 4c shows the stress–strain curves of materials with different D400 contents. The static

modulus, strength, and fracture strain data were calculated from the curves and summarized in Table 1. As the D400 content increases, the slope of the curve decreases, indicating a reduction in the material’s modulus. This is attributed to the significant increase in the length of molecular chain segments with increasing D400 content. Longer chain segments provide greater flexibility, enhancing the material’s deformation performance and resulting in a lower modulus at the macroscopic level. Meanwhile, the materials exhibit higher fracture strain values. Among them, DPS5 has the lowest Young’s modulus of 1 MPa, indicating elastic behavior (elastic: Young’s modulus between 0.1 and 10 MPa and high elongation > 200%<sup>[19]</sup>), while DPS1 has the highest Young’s modulus of 506 MPa, indicating rigidity. The modulus of the

**Table 1.** Fixing and recovery ratios for materials with different D400 ratios.

Sample no.	DPS1	DPS2	DPS3	DPS4	DPS5
Modulus [MPa]	505.9 ± 5.4	188.6 ± 2.0	50.5 ± 0.4	16.0 ± 0.1	1.6 ± 0.1
Strength [MPa]	22.1 ± 0.2	15.9 ± 0.2	8.5 ± 0.1	3.8 ± 0.1	2.0 ± 0.1
Elongation at break [%]	4.8 ± 0.1	9.4 ± 0.1	42.6 ± 0.4	63.1 ± 0.7	210.4 ± 3.9
$T_g$ [°C]	195	114	82	52	42

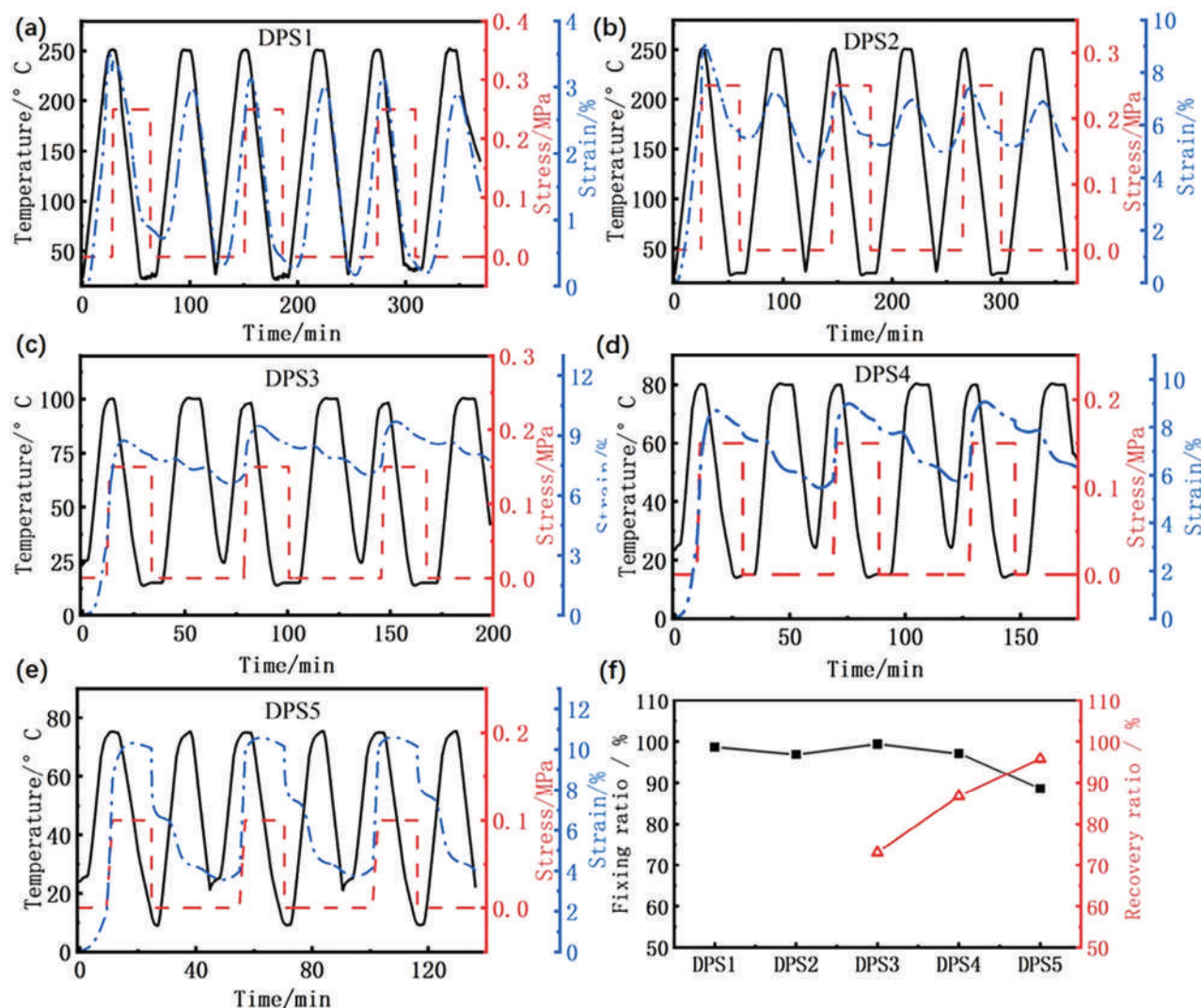


**Figure 5.** Three times consecutive shape memory cycles curves of a) DPS1, b) DPS2, c) DPS3, d) DPS4, e) DPS5; f) Fixing and recovery ratios for them.

highest modulus material is 506 times that of the lowest modulus material. In Figure 4d, the  $\gamma$ -axis scale for the modulus is in exponential magnitude, while the  $x$ -axis represents the D400 content of DPS1 – DPS5, which is consistent across the samples. With linear growth in D400 content, the modulus of the materials exhibits exponential growth. This indicates the significant influence of D400 on the modulus of the material system. As shown in Figure 4d (reaction scheme), D400 undergoes a Michael addition reaction with the bismaleimide group, where the amine reacts with the double bond of the bismaleimide group, converting the C=C double bond into a single bond while preserving the structure of the bismaleimide group. After the reaction between the bismaleimide group and the olefin, where the C=C double bond has already been converted into a single bond, its reaction with D400 leads to the cleavage of the single bond and the bismaleimide ring. The addition of D400 results in longer chain segments, and the cleavage of the bismaleimide ring leads to a more linear material system. Hence, the modulus of the material exhibits an exponential decrease.

The shape memory effect of the materials under a gradient temperature was verified by combining DPS2 – DPS5 together. The sheet-shaped materials were cut into flat shapes with four branches and each branch was bent 90 degrees at  $T_g + 6-34^\circ\text{C}$  and fixed at  $R.T.$ , as shown in Figure 6a. The four materials were then cut and shaped separately, and stacked on top of each other, with DPS5 at the bottom and DPS4-DPS2 stacked sequentially above, as shown in the middle of Figure 6. The temperature was gradually increased to the deformation temperature of each material, as shown in Figure 6b,e, and the structure unfolded at the transition temperature of each material. Finally, the structure recovered to its initial shape, as shown in Figure 6e. As shown in Figure 6b (Figure 6c,d are similar), due to the significant difference in the transition temperatures of different materials, when the preceding layer of material unfolded, the subsequent materials were able to maintain their shapes, achieving an ultra-wide ( $153^\circ\text{C}$ ) adjustable transition temperature.

Figure 7a shows the changes in disulfide bonds during the healing process of the tensile sample section. After the sample

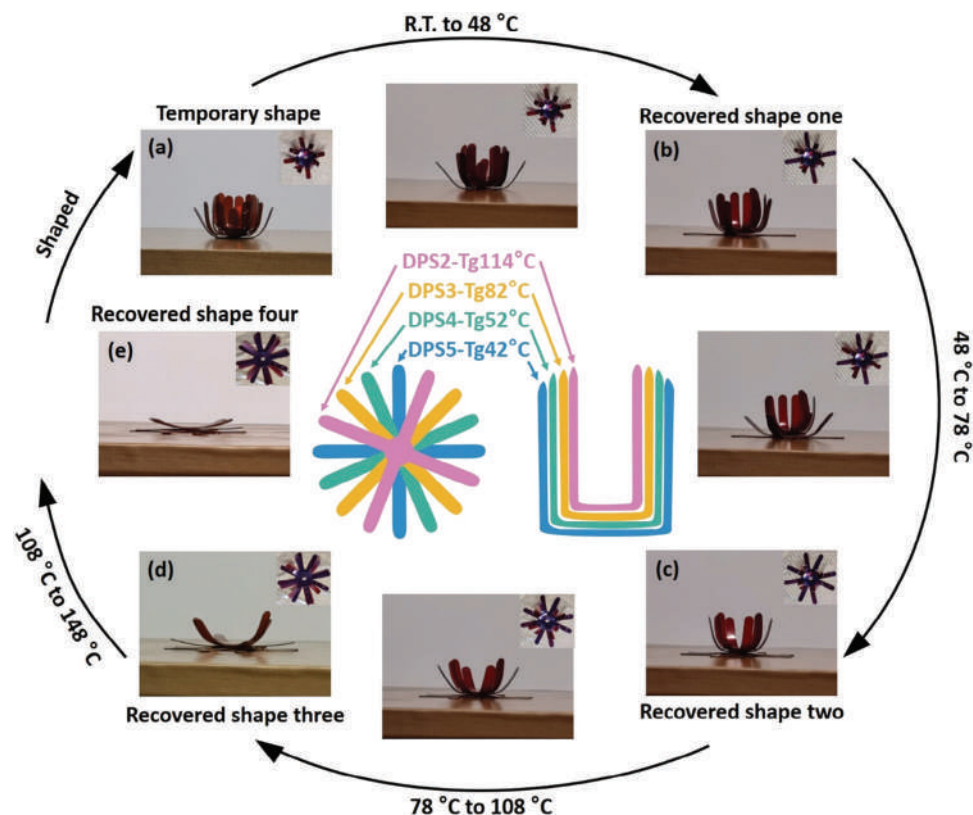


**Figure 6.** The structure composed of four materials undergoes the shape memory cycle process at four temperatures in sequence: a) A temporary structure composed of four materials at R.T.; b–e): Structures after deformation at four temperatures, which are 48, 78, 108, and 148 °C, respectively. The photos between (a) and (e) show the deformation process. From (e) to (a) is the process of shape fixing.

was cut, some disulfide bonds and some other molecular bonds on the surface of the section were break. When the sample was heated, the disulfide bond undergoes the exchange reaction, exhibiting the healing of the material in macroscopic. We conducted tensile tests on the healed SMPs and compared the test results with that of pristine SMPs, as shown in Figure 7b. The modulus and the elongation at break of the healed SMPs all decreased, indicating that while the material successfully healed, a portion of the molecular chains did not heal. The tensile properties of healed SMPs are summarized in Table 2. It can be seen that the higher the D400 content, the higher the modulus healing rate of SMP, reaching a maximum of 93.2%. As the lower the modulus, the longer and softer the molecular segments of SMP, the better the mobility of the molecular segments, and the more complete the healing process, demonstrating higher modulus healing rate. These SMPs all exhibit healing rate of

over 85% elongation at break, demonstrating good elongation healing rate. Figure 7c–l shows the photographs taken to verify the self-healing performance of the material. It can be seen that wedge-shaped cracks were cut from the surfaces of these SMPs, and wedge-shaped cracks disappearing after healing. It can be seen that these materials all have the function of self-healing. This is due to the introduction of disulfide bonds. During the heating process, the disulfide bond undergoes an exchange reaction, causing the fracture of materials to reconnect together. This study successfully achieved self-repair in thermosetting materials. When materials are used in some structure in space, once they are damaged, they can be repaired to restore their original mechanical properties and still have the function of shape memory. Moreover, we filmed the rapid self-healing process of DPS5 as shown in Video S1 (Supporting Information). The material returned to its original state immediately after being cut

**Table 2.** Tensile properties of healed SMPs and their healing rates.

Sample no.	DPS1-H	DPS2-H	DPS3-H	DPS4-H	DPS5-H
Modulus [MPa]	355.4 ± 12.8	147.5 ± 7.3	44.7 ± 4.2	13.8 ± 1.2	1.6 ± 0.1
Elongation at break [%]	4.3 ± 0.1	8.1 ± 1.3	38.3 ± 5.2	56.0 ± 4.8	179.1 ± 10.6
Healing rate of Modulus [%]	70.2	78.2	88.5	86.2	93.2
Healing rate of Elongation at break [%]	90.1	86.3	89.8	88.8	85.1

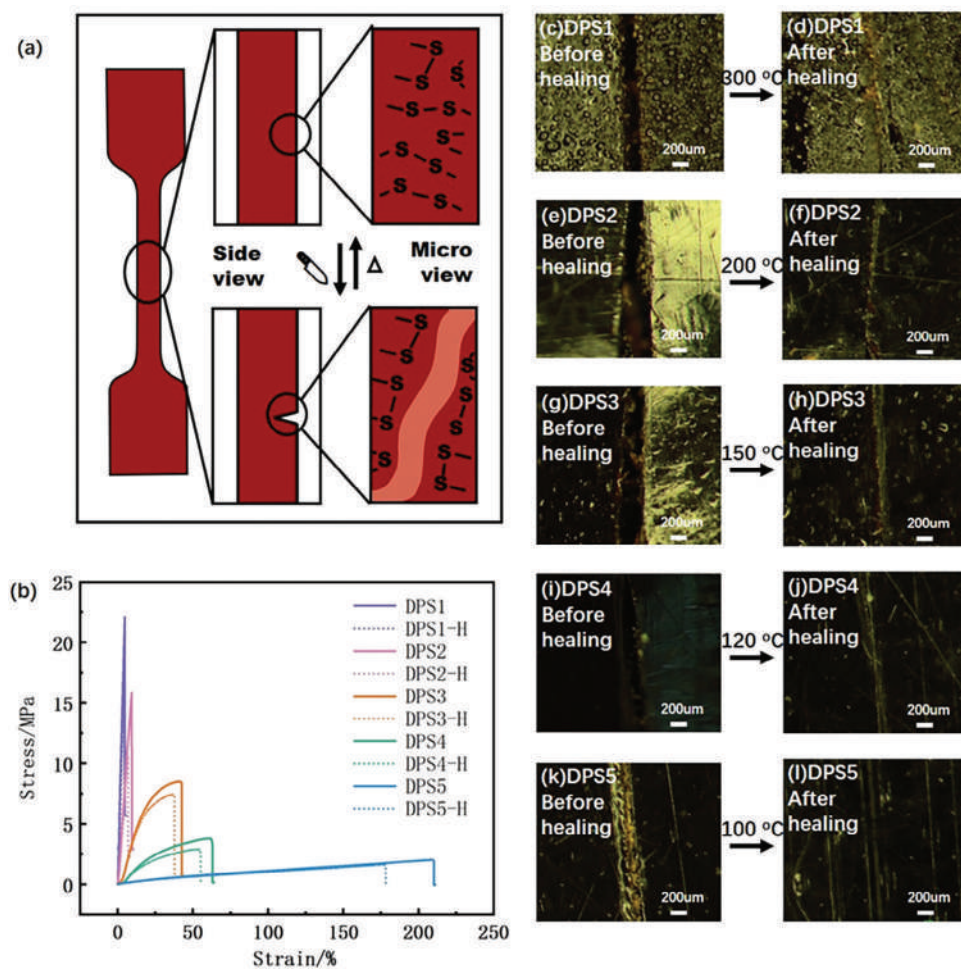


**Figure 7.** a) Changes in disulfide bonds during the healing process of the tensile sample section; b) Tensile stress–strain curves of healed SMPs compared with pristine SMPs; c–l) Microscopic graphs of self-healing process of SMPs; c,d): Graphs of DPS5 before and after healing; e,f): Graphs of DPS4 before and after healing; g,h): Graphs of DPS3 before and after healing; i,j): Graphs of DPS2 before and after healing; k,l): Graphs of DPS1 before and after healing.

on a heating table at 150 °C. The recycle process of shape memory bismaleimide space station structure is shown in **Figure 8a**. As a spatial deformable structure, when cracks and defects are present inside, the entire structure can be cut into pieces. The granular material can be reprocessed into its original structure through hot pressing, and the reprocessed structure can play its deformation role again in space structure again. The reprocessable performance of DPS5 was verified by hot pressing as shown in **Figure 8b,c**. Granular materials were squeezed together under pressure. The molecules at the edge of the particle moved in a heated state, and disulfide bonds undergo exchange reaction as well. In this way, the process of hot pressing caused the granular materials to connect with each other. The remold of thermosetting materials was realized. **Figure S6** (Supporting Information) shows the comparison of FTIR spectra of DPS5 before and after remolding, and the main characteristic peaks of the two are basically consistent, indicating that the remolding process has caused no change in the chemical structure of the material. **Figure S7** (Supporting Information) shows the stress–strain curves of DPS5 before and after remolding. It can be seen that the

material exhibits an increase in modulus and a decrease in elongation at break. This is due to the large proportion of long chains (D400) in DPS5. When the material is cut into small particles, more long chains break, while fewer short chains (BDM, S=S bond) break. After remolding, the D400 and BDM that fractured in DPS5 cannot recombine, manifested as a decrease in elongation at break and modulus of the material. But at this point, the modulus of the material increases. This is due to the fact that broken small molecules become gas and evaporate under heat and pressure, resulting in a shorter average chain length of the material. **Figure 8d** shows the deformation process of remolded bowknot structure of DPS5-R. The remold sheet DPS5 was cut and bent into a bowknot structure. When heated, the DPS5-R can still exhibit shape memory behavior, deforming into an unfolded bowknot structure. In space application scenarios, it is unrealistic to bring more materials into space for manufacturing. When there is significant damage or defect to the structure in space, the structure made of our material can be reshaped to have basic mechanical properties and still have the function of shape memory.

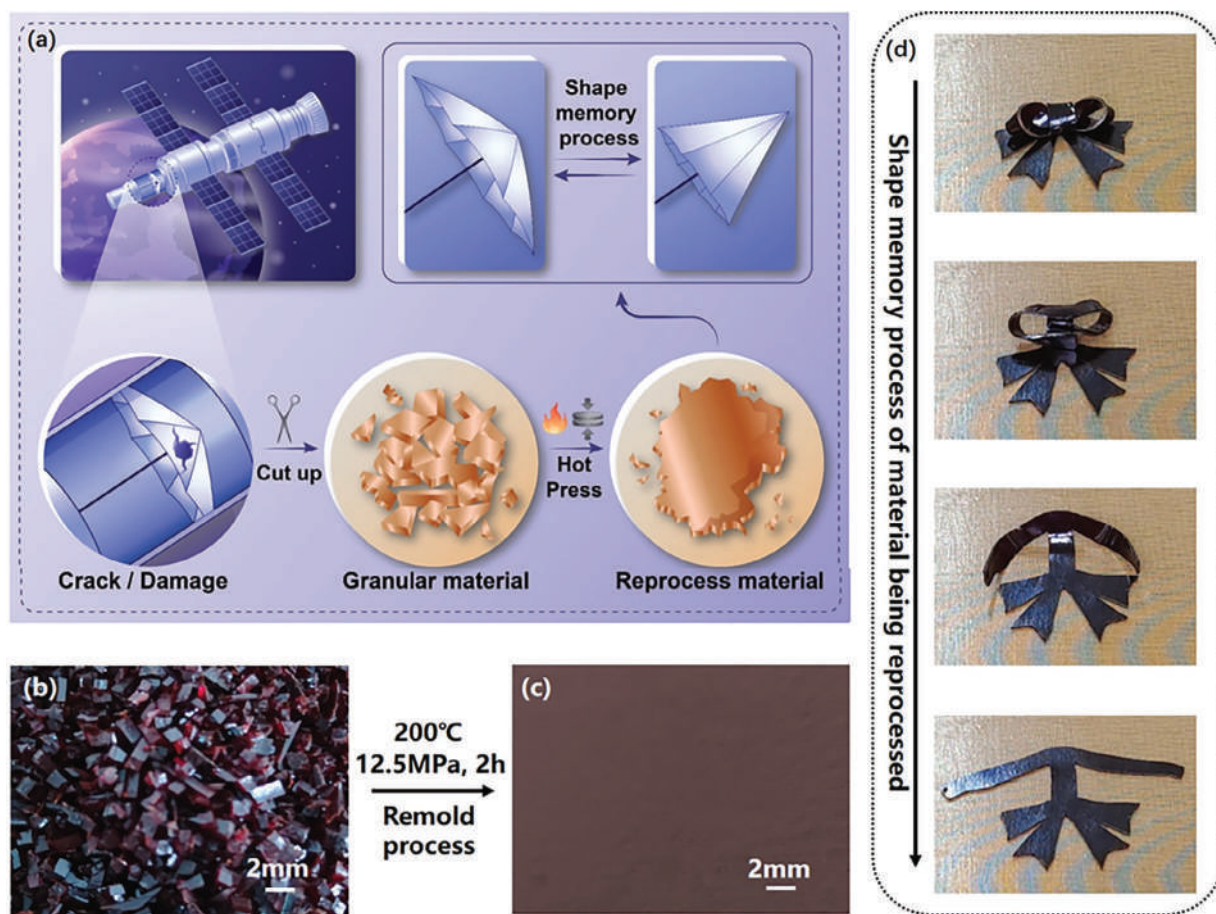


**Figure 8.** a) The schematic diagram of the recyclable shape memory bismaleimide space station structure, its recycle process after being damaged, and its shape memory process after remolding; b,c) Photos of DPS5 before and after remolding process; d) The deformation process of remolded bowknot structure of DPS5.

### 3. Conclusion

In response to the current limitations of thermosetting shape memory resins, such as their inability to be reshaped, ineffective realization of complex shape deformation, occurrence of microcrack damage during use, lack of harder materials in self-repairable systems, and absence of a series of compatible materials with significant hardness differences, we propose a thermosetting shape memory resin system capable of from ultra-soft to extremely hard with self-healing and reprocess functionality, along with its preparation method. Through the synthesis of material skeleton molecules that retain disulfide bonds while incorporating diene groups at both ends of the molecules, followed by the pre-polymerization of the diene groups with bismaleimide, a series of bismaleimide materials with shape memory effect were obtained. The fixing ratio and recovery ratio of these SMPs can reach 99.4% and 95.8%, respectively.

Subsequently, by introducing diamine molecules to adjust the crosslink density, we obtained the polymer series with adjustable modulus and a dynamic modulus exceeding three orders of magnitude at *R.T.* The dynamic modulus of the hardest material is 66 times that of the softest material, while the Young's modulus (static modulus) is 506 times higher, enabling an ultra-wide  $T_g$

range spanning 153 °C. The material exhibits a wide processing window during preparation, exceeding 50°C. Furthermore, materials possessing different moduli were integrated to create structures with variable stiffness and undergo deformation at different temperatures. Moreover, the incorporation of disulfide bonds into the synthesized olefin molecules helps to realize self-healing and reprocessable functionalities in thermosetting shape memory bismaleimide materials. Specifically, it achieved a healing efficiency of 93.2% of modulus and 90.1% of elongation at break. The shape memory bismaleimide can be remolded, and still perform deformation function after remolding. This significant advancement lays a solid foundation for the future recycling and reuse of aircraft, satellites, and other equipment, offering promising prospects for enhancing sustainability and efficiency within the aerospace industry.

### 4. Experimental Section

**Raw Materials:** DTDP, 98%, allyl bromide (98%), potassium carbonate ( $K_2CO_3$ , 99%), and BDM, 98% were commercially sourced from Shanghai Macklin Biochemical Technology Co., Ltd. Poly(propylene glycol) bis(2-aminopropyl ether) D-400 ( $D400$ ,  $M_w = 400 \text{ g}\cdot\text{mol}^{-1}$ ) was

obtained from Shanghai Aladdin Biochemical Technology Co., Ltd. Analytical grade acetone was procured from Sinopharm Chemical Reagent Co., Ltd. All chemicals utilized in the experiments were of analytical grade and were employed without any additional purification steps.

**Synthesis of DPS:** DTDP and allyl bromide were employed for the synthesis of DPS, as illustrated in Figure 1. The reaction was conducted in a three-necked flask under a nitrogen atmosphere at 50 °C. DTDP, anhydrous K<sub>2</sub>CO<sub>3</sub>, and acetone were combined and stirred in the flask. Subsequently, allyl bromide was added dropwise to the reaction mixture. The molar ratio of DTDP, allyl bromide, and anhydrous K<sub>2</sub>CO<sub>3</sub> was maintained at 1:3:4. After stirring the reaction mixture for 12 h, the resulting suspension was filtered to remove insoluble impurities. The filtrate, appearing as a bright yellow liquid, was subjected to rotary evaporation, yielding an amber-colored oily liquid identified as DPS with a yield exceeding 92%. Anhydrous K<sub>2</sub>CO<sub>3</sub> played a crucial role in promoting the reaction and establishing an alkaline environment. The subsequent treatment steps, including filtration and evaporation, effectively removed the generated by-products (potassium bromide, carbon dioxide, and water), resulting in the isolation of pure DPS.

**Preparation of Prepolymer and Cures Resins:** The DPS and BDM components were intimately mixed in a solvent-free manner, as illustrated in Figure 2. The mixture was subjected to a heating process at 150 °C for a duration of 30 min. During this period, BDM dissolved completely, resulting in the formation of a clear liquid. The mixture underwent a prepolymerization reaction, leading to the formation of linear oligomers. Subsequently, a specific amount of D400 was added to the mixture and stirred for 1–2 min until a homogeneous blend was achieved. The resulting uniform liquid was then poured into a preheated mold maintained at 150 °C, producing sheet materials with a thickness ranging from 0.5 to 1 mm. The mold utilized in the process consisted of two vertical glass plates held together by metal clips, with silicone strips measuring 0.5–1 mm in thickness sandwiched between the glass plates. Following the pouring of the liquid into the mold, a post-curing process was implemented. The post-curing procedure involved subjecting the samples to a temperature profile, including treatment at 150 °C for 2 h, followed by 180 °C for 2 h, and finally, 200 °C for 2 h (with the exception of DPS1, which was additionally subjected to a temperature of 220 °C for 1 h). After completion of the post-curing process, the samples were allowed to cool, and subsequently, they were carefully removed from the mold to prepare them for subsequent analyses. The molar ratios of DPS, BDM, and D400 utilized in the synthesis were as follows: 4:4:0, 4:4:1, 4:4:2, 4:4:3, and 4:4:4, resulting in the production of samples denoted as DPS1, DPS2, DPS3, DPS4, and DPS5, respectively.

**Materials Characterization Techniques <sup>1</sup>H and <sup>13</sup>C NMR:** The <sup>1</sup>H and <sup>13</sup>C NMR spectra were recorded using the INOVA-400 nuclear magnetic resonance instrument from Varian Company and the AgilentDD2-600 nuclear magnetic resonance instrument. CDCl<sub>3</sub> was employed as the solvent, while TMS served as the internal standard.

**FTIR Spectrometer:** The FTIR spectra were acquired using a Spectrum Two DGTS instrument (Perkin-Elmer, MA, USA) equipped with a universal attenuated total reflection accessory. This setup enabled the examination of molecular vibrations and the analysis of functional group interactions. The measurements were conducted within the wavelength range of 4000–650 cm<sup>-1</sup>, employing a spectral resolution of 4 cm<sup>-1</sup>.

**Rheology Analysis:** The rheological behavior of the materials was evaluated using a TA Instruments Waters LLC Rheometer equipped with 25 mm diameter parallel plate aluminum geometry. The plate-to-plate gap was set at 500 μm, and the temperature was ramped at a rate of 5 °C min<sup>-1</sup>. The measurements were conducted at an angular frequency of 6.28 rad s<sup>-1</sup> (1 Hz frequency).

**Swelling Test:** Crosslinking density is characterized by swelling test. About 0.2 g sample is weighed, with the weight recorded as *m*<sub>1</sub>. The weighed sample was put into sufficient deionized water or toluene. After two days, the solvent on the sample surface was wiped clean. The weight of dried sample was recorded as *m*<sub>2</sub>. Swelling degree is calculated by Equation (1).

$$\text{Swelling degree} = \frac{m_2 - m_1}{m_1} \times 100\% \quad (1)$$

**Thermal Analysis:** TGA was performed using a Mettler–Toledo TGA/DSC STARE System under a nitrogen (N<sub>2</sub>) flow environment. The samples were heated from 30 to 800 °C at a heating rate of 10 °C min<sup>-1</sup>. TGA provided valuable insights into the thermal changes and thermal stability of the SMPs. By monitoring the weight loss as a function of temperature, the decomposition and degradation behavior of the materials were characterized. Differential scanning calorimetry (DSC) measurements were conducted using a Mettler–Toledo DSC1 instrument under a nitrogen (N<sub>2</sub>) flow environment. The temperature range was set from 30 to 280 °C with a heating rate of 10 °C min<sup>-1</sup>. DSC analysis allowed for the determination of the approximate temperature at which the material begins to cure. By monitoring the heat flow as a function of temperature, the phase transitions, curing behavior, and thermal properties of the SMPs were evaluated.

**Mechanical Testing:** The static mechanical properties were evaluated using uniaxial tensile tests performed on a Zwick electronic universal material testing machine. The tests were conducted at *R.T.* with a crosshead speed of 1 mm min<sup>-1</sup>. ASTM-D638 Type-V standards were followed for testing pristine DPS1 – DPS5 samples. The dynamic mechanical properties of rectangular samples were assessed in tensile mode using DMA. The samples, with dimensions of 30 × 4 × 1 mm<sup>3</sup>, were subjected to a heating rate of 5 °C min<sup>-1</sup>. The samples were clamped using a tensile mode clamp. The DMA machine was used to perform consecutive shape memory cycles. The procedure involved heating the sample to *T*<sub>g</sub> + 30 °C, followed by heat preservation and stretching. While maintaining a tensile force of 4–8 N, the sample was cooled to *R.T.*, unloaded, reheated to *T*<sub>g</sub> + 30 °C, and finally cooled to *R.T.* to complete a cycle. Each sample underwent three cycles. The shape fixation rate (*R*<sub>f</sub>) was calculated using Equation (2), where *ε*<sub>fix</sub> represents the strain during shape fixation and *ε*<sub>deform</sub> represents the strain during deformation. The shape recovery rate (*R*<sub>r</sub>) was calculated using Equation (3), where *ε*<sub>recover</sub> represents the strain during shape recovery and *ε*<sub>initial</sub> represents the initial strain.

$$R_f (\%) = \frac{\epsilon_{fix}}{\epsilon_{deform}} \times 100\% \quad (2)$$

$$R_r (\%) = \frac{\epsilon_{deform} - \epsilon_{recover}}{\epsilon_{deform} - \epsilon_{initial}} \times 100\% \quad (3)$$

**Healing Process, Remolding Process, and Optical Microscopy Imaging:** The sample was placed on a heating table set at a temperature of *T*<sub>g</sub> + 6–34 °C. Using a blade, the surface of the sample was scratched to a depth of ≈0.5 mm. The scratched sample was then rapidly cooled and microscopic photos were taken. The photos before and after healing process were taken using an optical microscope. At the same time, a video of the scribing and response process was recorded. The samples after healing are named as DPS1-H to DPS5-H, respectively. ASTM-D638 Type-V standards were followed for testing healing DPS1-H to DPS5-H samples. The healing rate of them were obtained by dividing the modulus and elongation at break of DPS1-H to DPS5-H by the data of the pristine DPS1 to DPS5, respectively. For remolding, the sheet material was cut into triangular or square fragments with a side length of ≈1–2 mm. Stack the fragments together and clamp them in the middle with two steel plates covered with peel ply. The steel plate was heated at 200 °C and a pressure of 12.5 MPa was applied for two hours. The samples after remold are named as DPS5-R. The photos before and after remolding process were taken by mobile phone.

## Supporting Information

Supporting Information is available from the Wiley Online Library or from the author.

## Acknowledgements

The authors thank National Key R&D Program of China (2022YFB3805700) and National Nature Science Foundation of China (Grant No. 92271112) for the support of this work.

## Conflict of Interest

The authors declare no conflict of interest.

## Data Availability Statement

The data that support the findings of this study are available from the corresponding author upon reasonable request.

## Keywords

bismaleimide, reprocessable crosslinked polymers, self-healing materials, shape memory polymers

Received: August 22, 2023

Revised: November 9, 2023

Published online:

- [1] a) M. Behl, A. Lendlein, *Mater. Today* **2007**, 10, 20; b) J. Leng, X. Lan, Y. Liu, S. Du, *Prog. Mater. Sci.* **2011**, 56, 1077; c) G. Zhang, Q. Zhao, W. Zou, Y. Luo, T. Xie, *Adv. Funct. Mater.* **2016**, 26, 931; d) L. Yu, H. Yu, *ACS Appl. Mater. Interfaces* **2015**, 7, 3834; e) Y. Wang, S. Sun, P. Wu, *Adv. Funct. Mater.* **2021**, 31, 2101494; f) J. Lin, Y. Yu, Z. Zhang, F. Gao, S. Liu, W. Wang, G. Li, *Adv. Funct. Mater.* **2020**, 20, 1910479; g) Y. Li, H. Chen, D. Liu, W. Wang, Y. Liu, S. Zhou, *ACS Appl. Mater. Interfaces* **2015**, 7, 12988; h) D. Roy, J. N. Cambre, B. S. Sumerlin, *Prog. Polym. Sci.* **2010**, 35, 278; i) F. Zhao, X. Zheng, S. Zhou, B. Zhou, S. Xue, Y. Zhang, *Intel. J. Smart. Nano. Mater.* **2021**, 12, 72. j) Y. Li, W. Pan, F. Zhang, J. Leng, *J. Intel. Mater. Syst. Struct.* **2021**, 33, 1762. k) F. Zhao, X. Zheng, S. Zhou, B. Zhou, S. Xue, Y. Zhang, *Intel. J. Smart Nano Mater.* **2021**, 12, 72. l) H. Duan, J. Gu, H. Zeng, A. A. Khatibi, H. Sun, *Intel. J. Smart Nano Mater.* **2023**, 14, 243. m) P. Long, Y. Feng, C. Cao, Y. Li, J. Han, S. Li, C. Peng, Z. Li, W. Feng, *Adv. Funct. Mater.* **2018**, 28, 1800791.
- [2] a) Y. Li, F. Zhang, Y. Liu, J. Leng, *Comp. A* **2023**, 165, 107328; b) R. J. Iredale, C. WardCarwyn, I. Hamerton, *Prog. Polym. Sci.* **2017**, 69, 1.
- [3] H. Cao, R. Xu, D. Yu, *J. Appl. Polym. Sci.* **2008**, 109, 3114.
- [4] R. K. Jena, C. Y. Yue, M. M. Sk, K. Ghosh, *RSC Adv.* **2015**, 5, 79888.
- [5] P. Musto, E. Martuscelli, G. Ragosta, P. Russo, G. Scarinzi, *J. Appl. Polym. Sci.* **1998**, 69, 1029.
- [6] C. Gouri, C. P. Reghunadhan Nair, R. Ramaswamy, K. N. Ninan, *Eur. Polym. J.* **2002**, 38, 503.
- [7] a) D. Montarnal, M. Capelot, F. Tournilhac, L. Leibler, *Science* **2011**, 334, 965; b) K. Yu, P. Taynton, W. Zhang, M. L. Dunn, H. J. Qi, *RSC Adv.* **2014**, 4, 10108; c) J. P. Brutman, P. A. Delgado, M. A. Hillmyer, *ACS Macro Lett.* **2014**, 3, 607.
- [8] a) W. Denissen, G. Rivero, R. Nicolay, L. Leibler, J. M. Winne, F. E. Du Prez, *Adv. Funct. Mater.* **2015**, 25, 2451; b) A. Erice, A. Ruiz De Luzuriaga, J. M. Matxain, F. Ruipérez, J. M. Asua, H.-J. Grande, A. Rekondo, *Polymer* **2018**, 145, 127; c) A. Erice, I. Azcune, A. Ruiz De Luzuriaga, F. Ruipérez, M. Irigoyen, J. M. Matxain, J. M. Asua, H.-J. Grande, A. Rekondo, *ACS Appl. Polym. Mater.* **2019**, 1, 2472.
- [9] H. D. Stenzenberger, in: *Advances in Polymer Science*, Vol. 117 (Ed: P. M. Hergenrother), Springer, Berlin **1994**, pp. 90–181.
- [10] C. Nair, *Prog. Polym. Sci.* **2004**, 29, 401.
- [11] C. S. Sipaut, V. Padavettan, I. A. Rahman, R. F. Mansa, J. Dayou, M. Jafarzadeh, *Polym. Adv. Technol.* **2006**, 25, 673.
- [12] a) R. J. Morgan, E. Eugene Shin, B. Rosenberg, A. Jurek, *Polymer* **1997**, 38, 639; b) J. Hopewell, *Polymer* **2000**, 41, 8221.
- [13] V. R. Sastri, G. C. Tesoro, *J. Polym. Sci. C Polym. Lett.* **1989**, 27, 153.
- [14] G.-M. Wu, D. Liu, G.-F. Liu, J. Chen, S.-P. Huo, Z.-W. Kong, *Carbohydr. Polym.* **2015**, 127, 229.
- [15] Y. Zhang, H. Ying, K. R. Hart, Y. Wu, A. J. Hsu, A. M. Coppola, T. A. Kim, K. Yang, N. R. Sottos, S. R. White, J. Cheng, *Adv. Mater.* **2016**, 28, 7646.
- [16] M. Pepels, I. Filot, B. Klumperman, H. Goossens, *Polym. Chem.* **2013**, 4, 4955.
- [17] Y. Yao, M. Xiao, W. Liu, *Macromolecular* **2021**, 228, 2100002.
- [18] Y. Lai, X. Kuang, P. Zhu, M. Huang, X. Dong, D. Wang, *Adv. Mater.* **2018**, 30, 1802556.
- [19] G. Zhu, Y. Hou, N. Xia, X. Wang, C. Zhang, J. Zheng, D. Jin, L. Zhang, *Adv. Funct. Mater.* **2023**, 33, 2300888.
- [20] X. Chen, H. Lü, Q. Lin, X. Zhang, D. Chen, Y. Zheng, *J. Memb. Sci.* **2018**, 549, 12.
- [21] Y. Wang, L. Yuan, G. Liang, A. Gu, *Polymer* **2020**, 203, 122769.
- [22] M. Ozawa, M. Shibata, *React. Funct. Polym.* **2020**, 146, 104404.
- [23] C. Liu, H. Jia, N. Li, Y. Qiao, Z. Weng, G. Du, X. Jian, *Polym. Adv. Tech.* **2020**, 32, 1205.